THE IMAGE DISPLACEMENT INSTABILITY IN RADIAL LINE ACCELERATORS

B. B. Godfrey, R. J. Adler, M. M. Campbell, D. J. Sullivan
MISSION RESEARCH CORPORATION
1400 San Mateo Boulevard, S.E., Suite A
Albuquerque, New Mexico 87108

and

T. C. Genoni
Air Force Weapons Laboratory
Albuquerque, New Mexico 87117

Introduction

The radial line linear induction accelerator is a viable method for producing short pulse, high current, high energy electron beams. In the radial line accelerator, pulsed power technology is applied to an electron beam in series by a linear array of modules. The high voltage breakdown problems associated with pulsed power are then reduced because the electron beam is the only component affected by the full accelerating field. The primary difficulty encountered in producing intense beams from such linacs is beam stability.

We are interested in current levels useful for a variety of applications, including plasma heating[1], free electron lasers[2], simulation of radiation effects[3], and collective ion acceleration[4]. In particular, we note that the combination of high current and energy have been demonstrated to be extremely desirable for collective ion acceleration[5].

The instabilities in the accelerator fall into several categories. For azimuthal mode number $m \geq 1$ the diocotron[6] and resistive wall[7] instabilities occur. Nonlinear effects due to beam drift motion occur for all m values[8]. Zero frequency oscillations[9] and the Klystron instability[10] are m = 0 effects.

In this work we confine discussion primarily to the m = 1 instabilities induced by an accelerating (or nonaccelerating) gap in the drift tube, the beam breakup instability[11,12] and its zero frequency analog, the image displacement instability[13,14]. These instabilities are particularly dangerous in high current accelerators where they can rapidly amplify an initial small transverse displacement of the beam to such an extent that it strikes the drift tube wall.

Below, a recently constructed radial line accelerator is briefly described. The beam breakup and image displacement instability theories are then presented, and sample calculations indicating their rate of growth in various cases are given. We have experimentally observed the image displacement instability, and results from the experiment as well as from corresponding three-dimensional numerical simulations are discussed.

The RADLAC Accelerator

Figure 1 is a schematic of the 10 MeV, 30 kA RADLAC accelerator developed jointly by the Air Force Weapons Laboratory and Sandia National Laboratory. The center conductor of each line is charged by a Marx generator to 3 MeV. When a cavity switch is closed, the full voltage appears across one side of the line only (for 12 ns in RADLAC). Sequentially triggering the radial lines accelerates the passing beam to its final high energy.

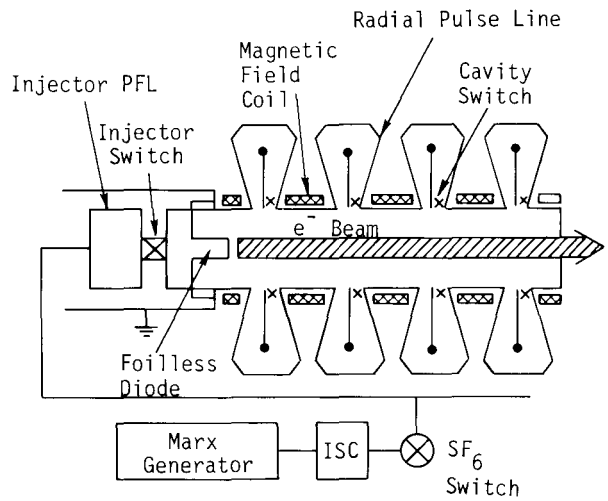

Figure 1. Schematic design of the RADLAC accelerator.

In order that the beam current be well below the spacecharge limit in the accelerator drift tube, the electron beam is injected at 2 MeV and with an annular crossection. Focusing is provided by a solenoidal magnetic field, $B_z \sim 10$ kg.

Instability Theory

Several simplifying assumptions are invoked to reduce the beam transverse dynamics to a tractable form. Each axial segment of the beam is assumed to displace rigidly in the transverse direction, and the displacement is taken to be small compared to the drift tube radius, b. In turn, the drift tube radius is much smaller than the betatron wavelength, $\lambda_c = 2\pi\gamma mc^2/eB$. The beam axial velocity is $v \approx c$, with $\gamma \equiv (1 - v^2/c^2)^{-\frac{1}{2}} \gg 1$. Any axial relative displacement of the beam segments is ignored.

With $\xi = x + iy$, the equation of transverse motion for the beam centroid is found to be

$$\frac{\partial}{\partial z}\gamma\frac{\partial}{\partial z}\xi - i\omega_c\frac{d}{d\xi}\xi = \frac{2I_e}{b^2mc\gamma^2}$$

$$+\sum_j \delta(z - z_j)\left(\frac{2I_e f_\ell}{mb^2c}\xi + \frac{ieB_{j\ell}}{c}\right) \qquad (1)$$

Note that B_j excludes the image displacement portion of the magnetic field, which is the $2Ief/mb^2c$ term. B_j is the transverse magnetic field of a single TM1n0 mode of the accelerating cavity in the jth gap at frequency ω and quality factor Q. The gap width is ℓ. The growth of B_j can be derived from a cavity normal mode relation with the source resulting from an off-axis beam:

$$\frac{d^2B_j}{dt^2} + \frac{\omega}{Q}\frac{dB_j}{dt} + \omega^2 B_j = i\frac{Z_\perp \omega^3 I \xi(z_j)}{Q\ell c} \qquad (2)$$

We note that both $\xi(z_j,t)$ and $I(t)$ have Fourier components at frequency ω.

Several constants are built into the structure of equations (1,2). The image displacement force constant f measures the ratio of the transverse force in the gap to the transverse electric force in the drift tube. It is typically of order ~ 1/2. The accelerating gaps do not have to be resonant for reasons of efficiency, in contrast to those of RF linacs. However, the requirements for voltage standoff, power feeds, etc., result in enough wave reflections to justify modeling the gap regions as a lossy cavity. Thus, $Z_\perp$ (the cavity transverse impedance) and Q must be found. Given these constants and the initial time dependence of I and ξ, a complete linear description is defined.

We must estimate the growth of these instabilities in order to design future accelerators. To do this, equations (1) and (2) have been integrated numerically for a few sets of idealized conditions.

The image displacement results for a 100 kA beam are summarized in Table I. The effect of a small change in focusing magnetic field can be very large in terms of instability growth, as illustrated by cases 1-5 and 6-7. In all cases, the effect of acceleration is to reduce growth . Even with acceleration, however, a resonance in growth as a function of B_z is observed in case 6. Case 2 illustrates a prohibitively large growth of $1600(2.1^{10})$ for 10 nonaccelerating gaps.

For long accelerators with greater than 15 gaps, beam breakup dominates over image displacement. For a 10-gap, 50 kA accelerator beam breakup computation results are summarized in Table II. It is important to note that the growth rates listed in the table apply only to a perturbation due to a fast rise-time beam displaced by a constant amount. The frequency component resonant at frequency ω is much smaller. The measurement of the parameters $Z_\perp/Q$ and Q is summarized elsewhere[17] -- these values are characteristic of radial line accelerators.

Acceleration reduces the growth rate by up to a factor of 20 for the parameters considered here. Further reductions in growth are expected if the effects of finite current and voltage rise time are also included.

Table I. Calculated Image Displacement Instability Growth

Case	B_z (kg)	(ℓ/b^2) (cm-1)	Γ
1	20.0	0.8	7.5
2	19.88	0.8	1600.0
3	19.74	0.8	340.0
4	19.01	0.8	2.4
5	19.47	0.8	2.2
6	20.0	0.8	470.0
7	20.46	0.8	48.0
8	20.0	0.29	4.5
9	19.83	0.29	7.3
10	20.46	0.29	1.6

Cases 1-5 are without acceleration, and cases 6-10 include acceleration at the gaps. Γ is the growth for ten gaps.

Table II. Calculated Beam Breakup Instability Growth

Case	B_z (kg)	$Z_\perp/Q$ (ohm)	Q	τ_R (cm)	Γ
1	20.0	20	10	0	7.0
2	20.0	20	20	0	350.0
3	20.0	40	10	0	700.0
4	20.0	20	10	0	3.3
5	20.0	40	10	0	35.0
6	19.83	20	10	0	4.2
7	19.66	20	10	0	3.1

Γ is the total instability growth for 10 gaps relative to the initial displacement. Cases 4-7 include acceleration effects.

Image Displacement Experiment

An experiment has been performed in a nonaccelerating structure to investigate the image displacement effect. It addresses several of the issues not included in the simple theory of the last section, particularly short wavelength effects. A side view of the experimental structure is shown in Figure 2. Nonaccelerating gaps were used in the experiment so that the size and cost of the experiment could be minimized.

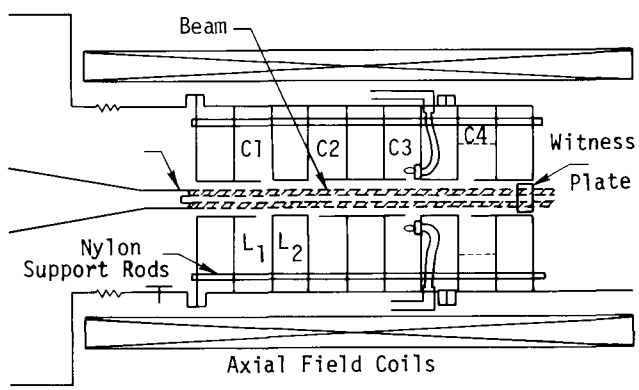

Figure 2. Side view of a typical image displacement simulation structure.

The foils shown in Figure 2 suppressed competing instability effects, including beam breakup and zero frequency radial oscillations. The m = 1 magnetic field penetrates through the foil in less than a nanosecond, and the defocusing electric field is increased by a factor of ~2.

In a periodic configuration the momentum changes due to each gap will always add in phase for $\lambda \sim L$ where L is the distance between gaps. Thus, if we vary λ we expect to see resonances for $n\lambda = L$ where n is an integer. The obvious method of diagnosing the experiment is the use of magnetic loop pairs. However, for the parameter regime $\lambda \sim b$, these underestimate the beam offset. Witness plates (i.e., the damage of a target in the beam path due to the beam) are a less accurate alternative method. They have the disadvantage of registering a pattern which is a complicated function of the beam energy deposition. A particular difficulty of witness plates is that they may not detect differences between the magnetic and geometric beam centroids.

The beam offset as a function of magnetic field for the geometry of Figure 2 is shown in Figure 3, where the dots depict the experimental points, and the solid curve is the linear theory corrected for finite gap effects and spatial transients.

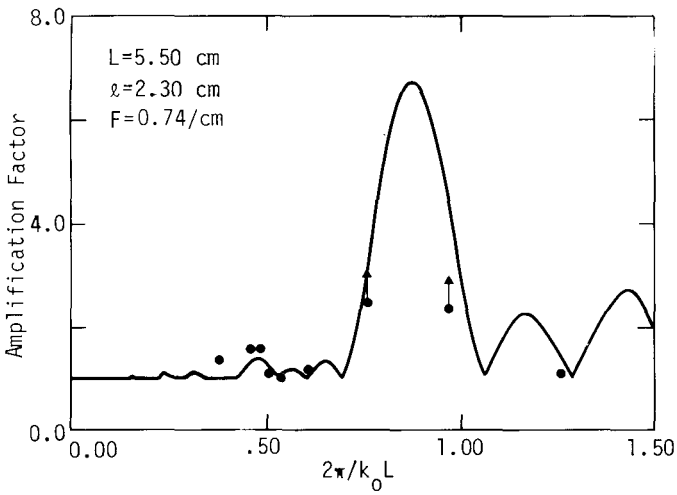

Figure 3. Comparison of linear theory and experimental image displacement amplification. The two vertical lines indicate that those points are lower bounds.

The points attached to a vertical line are of particular interest -- they indicate that the beam was so poorly defined that only a lower bound on the offset was available. This, we believe, is the first experimental observation of the instability.

A second effect was observed with magnetic probes. The beam drifts in θ through the gaps at a frequency $\sim(B_\theta(b)/B_z)(c/b)$, where $B_\theta(b)$ is the beam self-field measured at the drift tube wall.

An experimental configuration similar to that of Figure 2 was studied with the three-dimensional particle-in-cell simulation code IVORY. Typical code results are shown in Figure 4 for an axial magnetic field somewhat lower than achievable in the

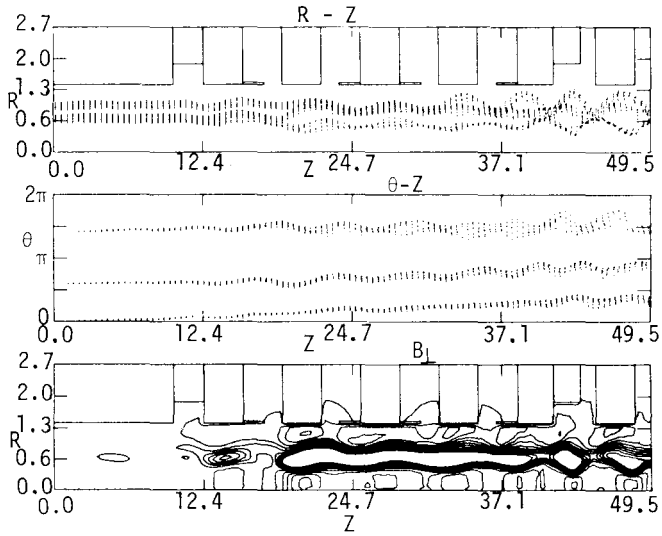

Figure 4. R(Z), θ(Z) particle plots and $B_\perp$ contours of a 3-D simulation run. Three streamlines are shown.

experiment. The plots of particles in the r-z and θ-z planes are shown. The θ-z plots indicate the particle drift while the three r-z particle streamlines indicate the resonant particle betatron motion, and mixing of the azimuthally symmetric and image displacement oscillations. We anticipate that this new code will be a powerful tool in the study of collective particle effects in intense beams.

Acknowledgement

This research was supported by the U. S. Air Force Weapons Laboratory. We are endebted to R. B. Miller for valuable discussions.

References

1. L. E. Thode, Phys. Fluids 19, 831 (1976).
2. V. L. Granatstein et al, Appl. Phys. Lett. 30, 384 (1977).
3. T. H. Martin, IEEE Trans. Nuc. Sci. NS-16. 59 June 1969.
4. R . Adler, J. A. Nation and V. Serlin, Phys. Fluids 24, 347 (1981).
5. R. Adler, J. Appl. Phys. 52, 3099 (1981).
6. M. E. Jones and M. A. Mostrom, J. Appl. Phys. 52, 3794 (1981).
7. B. B. Godfrey, unpublished.
8. J. W. Poukey, unpublished.
9. T. C. Genoni, M. R. Franz, B. G. Epstein, R. B. Miller and J. W. Poukey, J. Appl. Phys. 52, 2646 (1981).
10. J. G. Siambis and M. Friedman, Part. Accel. 8, 217 (1978).
11. W. K. H. Panofsky and M. Bander, Rev. Sci. Inst. 39, 206 (1968).
12. V. K. Neil, L. S. Hall and R. K. Cooper, Part. Accel. 9, 213 (1979).
13. C. H. Wood, Rev. Sci. Inst. 41, 959 (1970).
14. V. K. Neil, LLNL Report UCID-17976, Nov. 1978.
15. R. B. Miller, et al, J. Appl. Phys. 52, 1184 (1981).
16. J. A. Nation and M. E. Read, Appl. Phys. Lett. 23, 429 (1973).
17. R. J. Adler, T. C. Genoni, and R. B. Miller, IEEE Trans. Nuc. Sci. NS-28, 3467 (1981).